

Damage classification of concrete structures based on grey level co-occurrence matrix using Haar's discrete wavelet transform

Shahid Kabir[†] and Patrice Rivard[‡]

*Groupe de Recherche sur l'Auscultation et l'Instrumentation (GRAI),
Department of Civil Engineering, Université de Sherbrooke, Québec, J1K 2R1 Canada
(Received September 8, 2006, Accepted July 6, 2007)*

Abstract. A novel method for recognition, characterization, and quantification of deterioration in bridge components and laboratory concrete samples is presented in this paper. The proposed scheme is based on grey level co-occurrence matrix texture analysis using Haar's discrete wavelet transform on concrete imagery. Each image is described by a subset of band-filtered images containing wavelet coefficients, and then reconstructed images are employed in characterizing the texture, using grey level co-occurrence matrices, of the different types and degrees of damage: map-cracking, spalling and steel corrosion. A comparative study was conducted to evaluate the efficiency of the supervised maximum likelihood and unsupervised *K*-means classification techniques, in order to classify and quantify the deterioration and its extent. Experimental results show both methods are relatively effective in characterizing and quantifying damage; however, the supervised technique produced more accurate results, with overall classification accuracies ranging from 76.8% to 79.1%.

Keywords: damage detection; grey level co-occurrence matrix; multi-resolution analysis; supervised and unsupervised classification; wavelet transform, cracking.

1. Introduction

Concrete bridge deck deterioration is a significant problem that must be addressed to preserve highway infrastructure investments in bridges around the world (Scott, *et al.* 2003). Virtually all bridge decks will fail to serve out their service-lives (Bettigole and Robinson 1997), as they become increasingly susceptible to various types of deterioration due to challenging environmental conditions and increased traffic volumes. Weathering of concrete surfaces by wind, rain, snow, or mechanical actions caused by temperature-related expansion and contraction of surface moisture can result in the gradual wearing away of the concrete surface, otherwise known as erosion. Chloride-induced corrosion occurs when reinforcing steel has been placed too close to the surface of the concrete, or has been exposed by spalling, erosion, or cracking; the steel oxidizes in the presence of salt-rich moisture causing a loss of surface bonding between steel and concrete, which reduces the unified effect of reinforced concrete to resist tensile and compressive forces. The loss of surface concrete in pieces of various sizes is called spalling and is caused when expansive forces inside and near the

[†] PhD Candidate, E-mail: shahid.kabir@usherbrooke.ca

[‡] Associate Professor, Corresponding Author, E-mail: Patrice.Rivard@usherbrooke.ca

surface of concrete act along a weak plane or create a weakened plane; the expansive forces can be attributed to stress related to the corrosion of reinforcing steel or imbedded metal items, or the expansion and contraction of moisture, trapped inside the matrix of the concrete and absorbed by porous aggregates, in thermal cycles. Concrete surface cracks with a distinctive map-like pattern are usually the result of the alkali-aggregate reaction, which is one of the most common causes of concrete deterioration in several countries around the world, and especially in Eastern Canada (Fournier and Bérubé 2000); other types of cracks may be related to structural overloading, foundation settling, inherent design flaws, or other harmful conditions.

One major problem facing bridge management is the excessive costs required for the maintenance, replacement, rehabilitation or repair of bridge decks. Although traditional visual bridge inspection methods may be effective in many cases, the lack of objective and quantitative information provided by such evaluations can lead to significant differences between the estimated and the actual condition of a bridge, and the quantity of repair work required. These approaches are also costly, time-consuming, and often a disruption to traffic.

Imaging techniques are increasingly being used in the evaluation of concrete structures. The objective of imaging methods is to improve the qualitative visual analysis of image data with a quantitative analysis through automated identification of features in the image. This is desired because a computer can discriminate and analyze at the pixel level, and can examine and identify as many pixels as needed, thus taking full account of the spatial and spectral details present in the image (Schowengerdt 1997). Automated interpretation of images is considered a quantitative analysis due to its capacity to identify pixels based on their numerical properties and to provide area estimates by counting pixels. It is also generally called classification, which is a method where labels are attached to pixels according to their spectral characteristics by a computer that is trained beforehand to recognize pixels with similar spectral properties (Richards and Jia 1999). As a result, these methods can enhance visual inspections by providing quantitative information about the deterioration, including the location and the extent of damage, as well as by reducing the cost and time involved.

There is, however, a need for the development of effective image analysis methods in order to convert the information contained in the images into a more useful format for damage assessment. Conventional multispectral image analysis techniques are based on the spectral information present in the image, which is adequate for the classification of spectrally homogeneous object classes, such as newly-paved asphalt. Consequently, for applications involving the heterogeneous features found in concrete images, results obtained from such methods are inadequate. This is mainly because the contribution of spectral information is limited since heterogeneous objects are distinguished better through their spatial properties rather than their spectral properties (Kiema 2002). Another significant drawback of these conventional spectral approaches is that while the information content of the imagery increases with spatial resolution, the accuracy of the classification may decrease (Shaban and Dikshit 2001). This is due to increasing spectral variability within the classes, inherent in more detailed, higher spatial resolution images.

2. Scope of work

Statistical texture methods analyze the spatial distribution of grey values in an image by computing local features at each point in the image, and deriving a set of statistics from the

distributions of the local features. Texture analysis is a potential source of unique information to supplement spectral data in order to overcome the obstacles of spectral analysis of high resolution imagery (Kabir, *et al.* 2006). In the past, one difficulty concerning texture analysis was the lack of adequate tools to characterize different scales of texture effectively; texture classification based on statistical methods have been successful in many fields but are limited since they focus primarily on the relationship of image pixels on a single scale. Some textures are hierarchical, composed of nested texture elements that are only visible according to the scale of perception, or resolution. Also, many images contain textures that are not pure, with non-uniform backgrounds that are usually at a different scale. However, developments in spatial-frequency analysis, such as wavelet transforms, have provided good multiresolution analytical techniques, which have aided in resolving this obstacle. Wavelet transforms are mathematical tools capable of decomposing functions, and sorting digital signals, such as images, into scale-specific information.

This study proposes the application of Harr’s wavelet transform signal processing, along with grey-level co-occurrence matrix statistical texture analysis, on images depicting various types of concrete damage, in order to extract spatial information to be combined with spectral data in the classification approach, for improved characterization and quantification of the different types of damage in concrete imagery. A comparative study was conducted to evaluate the efficiency of the supervised maximum likelihood and unsupervised *K*-means classification techniques, which were used to classify and quantify the deterioration in the concrete and its extent.

3. Concrete specimens

3.1. Laboratory specimens: CANMET and GRAI

In this study, two sets of concrete specimens that were made in the laboratory with varying mixture proportions were investigated (Table 1). All exhibited various levels of surface cracking associated with alkali-aggregate reaction (AAR), which is a deleterious reaction between aggregates containing siliceous phases and alkali hydroxides in the concrete pore solution.

One set is composed of three concrete blocks, measuring 40 cm × 40 cm × 70 cm in size, and referred to as C1, C2, and C3. Concrete was batched with a reactive limestone as coarse aggregate, and blocks were left to the elements for over ten years at the CANMET site (Ottawa, Canada).

Table 1 Concrete mixture proportions and test measurements of specimens

Concrete Mixtures	CANMET			GRAI		
	C1	C2	C3	G1	G2	G3
Density (kg/m ³)	2303	2303	2317	2223	2326	2340
Cement content (kg/m ³)	423	423	425	210	390	390
Total Na ₂ O _{eq} (kg/m ³)	1.69	3.81	5.31	3.81	3.25	5.25
W/C	0.42	0.42	0.42	0.75	0.66	0.66
Test Measurements						
Average <i>P</i> -wave velocities (m/s)	4909	4513	4402	3810	3590	3440
Average expansion (%)	0.025	0.283	0.340	0.000	0.060	0.100

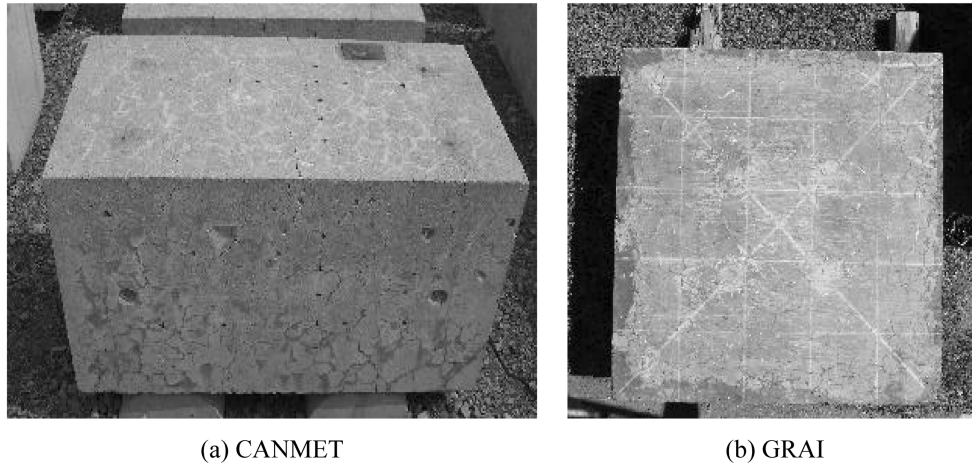


Fig. 1 Laboratory specimens

The other set contains three concrete slabs that measure $100\text{ cm} \times 100\text{ cm} \times 25\text{ cm}$ in size. Slab G1 was made with a non-reactive aggregate, while G2 and G3 were made with a reactive limestone. After concrete hardening, the slabs were wrapped in damp terry cloth and stored at ambient air ($20 \pm 2^\circ\text{C}$), at the GRAI laboratory at the University of Sherbrooke (Québec, Canada). Examples of the specimens are given in Fig. 1.

AAR leads to swelling and cracking in concrete, the amount of which is closely related to the expansion level and other indicators of concrete deterioration, such as loss of rigidity, decreasing mechanical properties, etc. (Rivard, *et al.* 2005). Consequently, tests were carried out on the CANMET and GRAI specimens in order to estimate the amount of inner damage. It is known that compression (P) wave velocities decrease with increasing amount of damage (Carino 2003). Therefore, P -wave velocities were measured through the Impact-echo method. Expansion was measured using stainless steel studs that were fixed on the top surfaces and on the sides of the specimens. Details about the average expansion levels and P -wave velocities of the specimens are given in Table 1.

3.2. Field samples

Various bridge components from six different bridges, located in Montréal and Sherbrooke (Southern Québec, Canada), were selected for this research, due to the varying types and degrees of concrete damage they manifest. Some of the bridge components are located at the St. Lambert Lock in Montréal, Québec, which is part of the St. Lawrence Seaway, and is severely affected by AAR, with various rates of concrete swelling (Gaudreault 2003). Greyscale images were employed, presenting four types of concrete damage: cracking, spalling, corrosion of reinforcement steel, and erosion (Fig. 2). Images were taken by digital camera with an image dimension of 1024×1024 pixels.

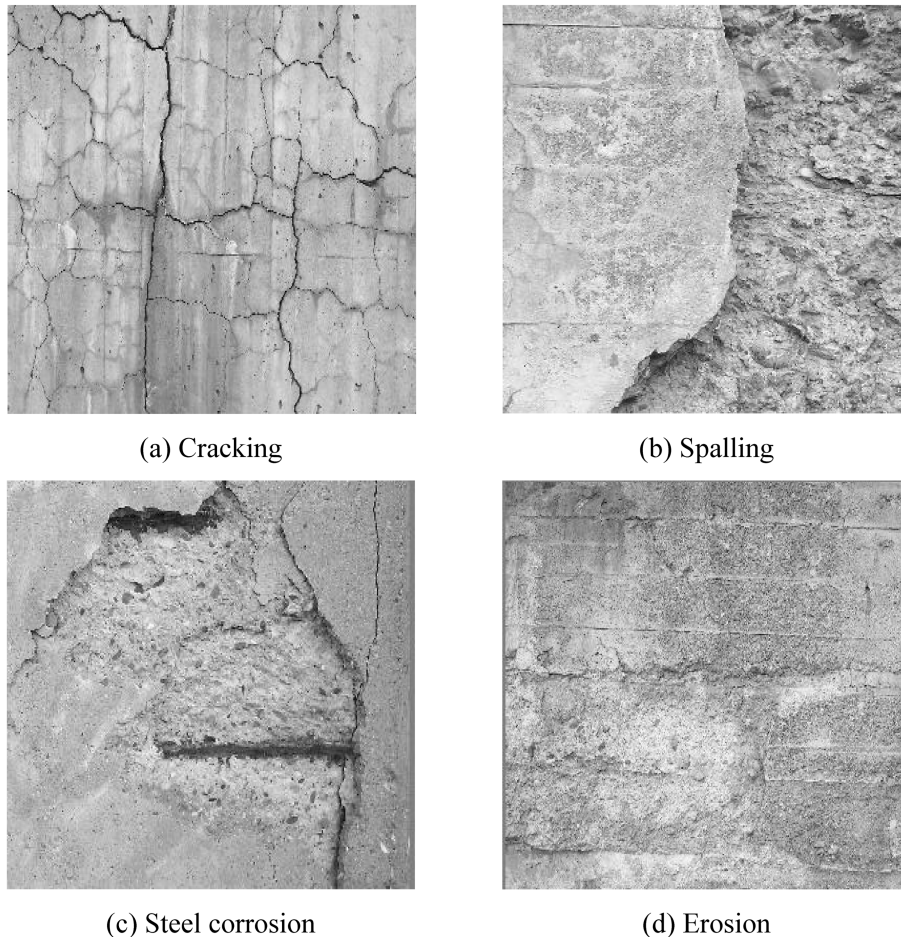


Fig. 2 Examples of damage in laboratory specimens and bridge components

4. Haar's discrete wavelet transform

The wavelet transform allows a signal to be converted and manipulated while keeping resolution across the entire signal and still be based in time. Wavelets are finite windows through which a signal can be viewed; in order to move the window about the length of the signal, the wavelets can be translated about time in addition to being compressed and expanded. Haar's transform is the simplest form of wavelets; it is essentially a process of averaging and differencing of values.

For two-dimensional images, the discrete wavelet transform (DWT) is applied to the pixel values in each row of the digital image, then to each column. In a pyramidal decomposition, an image is scaled into one low-resolution image (LL_1), which corresponds to coarse-scale coefficients, and three detail images (LH_1 , HL_1 and HH_1), which represent the fine-scale coefficients, thus producing a set of four sub-band images, as in Fig. 3(a). The low-resolution image can further be decomposed into the next level of low-resolution and detailed images. Therefore, depending on the number of resolution steps required $1, 1+3^1$ sub-band images will be produced, resulting in a multi-level decomposition as shown in Fig. 3(b). In this study, Harr's wavelet transform was applied on all of

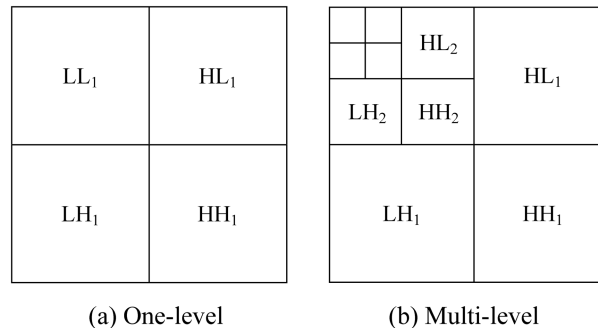


Fig. 3 Pyramidal wavelet decomposition

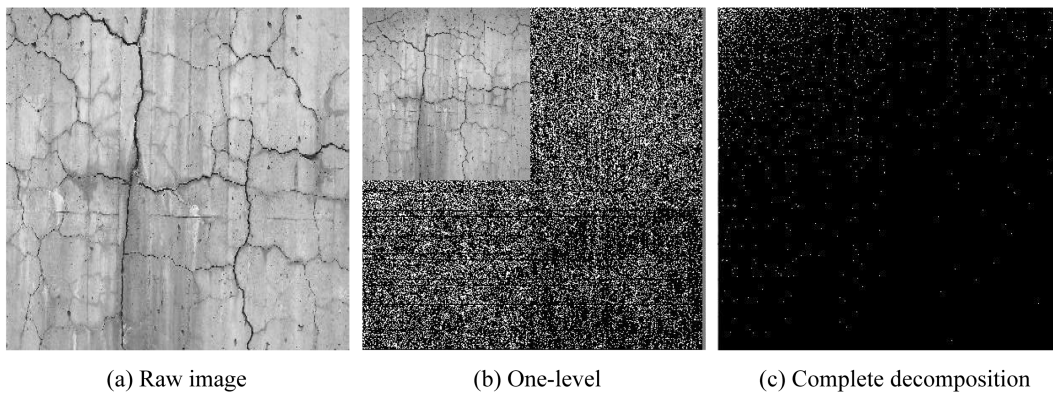


Fig. 4 Image decomposition

the greyscale images.

An original greyscale image sample of a bridge component with a high level of cracking is seen in Fig. 4(a), with all texture information present. Fig. 4(b) shows a one-level pyramidal decomposition of the image, resulting in four sub-band images, where the low-resolution image appears in the top left-hand corner surrounded by the three detail images. Fig. 4(c) is the full decomposition, which required ten resolution steps since the image resolution was 1024×1024 pixels ($2^{10}=1024$).

In order to exploit the texture information isolated in the decomposed components of the image, the components are assembled back into the original image at various levels of reconstruction, using the inverse discrete wavelet transform (IDWT). The wavelet coefficients obtained from decomposition are upsampled and filtered. This process filters out or minimizes the unwanted textures, which are often naturally present, or which may result due to varying surface conditions, such as moisture content, temperature, discolouration, surface roughness, etc.

After decomposition of the input images, the resulting detail images were used to produce reconstructed images for each input image; these reconstructed images contain the fine details, such as narrow cracks, wide cracks, and spalling damage. Images reconstructed to various levels are presented in Fig. 5. For the purposes of this study, the 25% reconstructions, an example of which is seen in Fig. 5(d), were employed because these images demonstrate how most of the unwanted texture, also known as background noise, has been removed by the wavelet transform leaving the

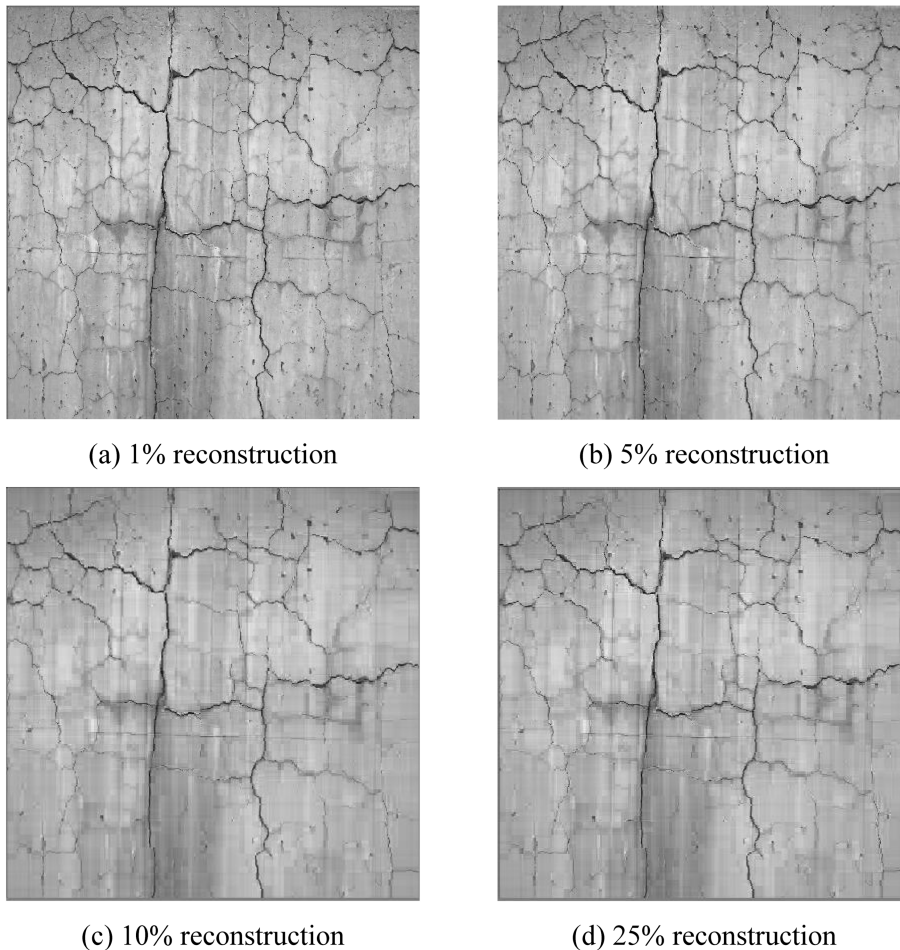


Fig. 5 Image reconstruction

finer details, which in this case are the cracks in the concrete surface.

5. Grey level co-occurrence matrix

One of the defining qualities of image texture is the arrangement of the grey values in the image space, known as the spatial distribution. Statistical texture methods analyze the spatial distribution of grey values by computing local features at each point in the image, and deriving a set of statistics from the distributions of the local features. Second-order statistics operate on a probability function that measures the probability of observing a pair of grey values, separated by a certain distance and direction, occurring in the image. This probability function, referred to as a second-order histogram, is also known as the grey level co-occurrence matrix (GLCM), as it measures the probability of the co-occurrence of two pixel values. Since the GLCM expresses the two-dimensional distribution of pairs of grey-levels, it can be considered a summary of the spatial and spectral frequencies of the image.

Texture analysis rarely uses individual properties of the statistics. Instead, statistical features are

derived for the extraction of textural information from the image. These features are obtained through processes that take measured grey values to compute new values. In the case of second-order statistics, the grey values in a pixel window of specific size are taken and the result of the computations is written back on the central pixel. The process is repeated for all pixels in the image. The outputs of the derived features are images in which the pixel values have been changed to reflect a particular feature, or texture; the resulting feature images are known as texture features.

5.1. Selection of pixel distance and direction

The success of the GLCM method depends on the choice of the distance and the direction between pixels. The appropriate distance between pixels depends on how fine or coarse the texture of interest is; small distances are usually used for fine textures while greater distances are generally used for more coarse textures. Small distances, though, are appropriate for textures that are fine, as well as coarse. As a result, one pixel distance was used in this study.

Concerning the direction between pixels, four directions can be used: 0° (horizontal), 45° (diagonal), 90° (vertical) and 135° (diagonal). The most common choice for the direction between pixels found in literature, however, is 0°, which was employed in this study also.

5.2. Selection of appropriate window

The effectiveness of the GLCM also depends on the size of the pixel window used. If the window

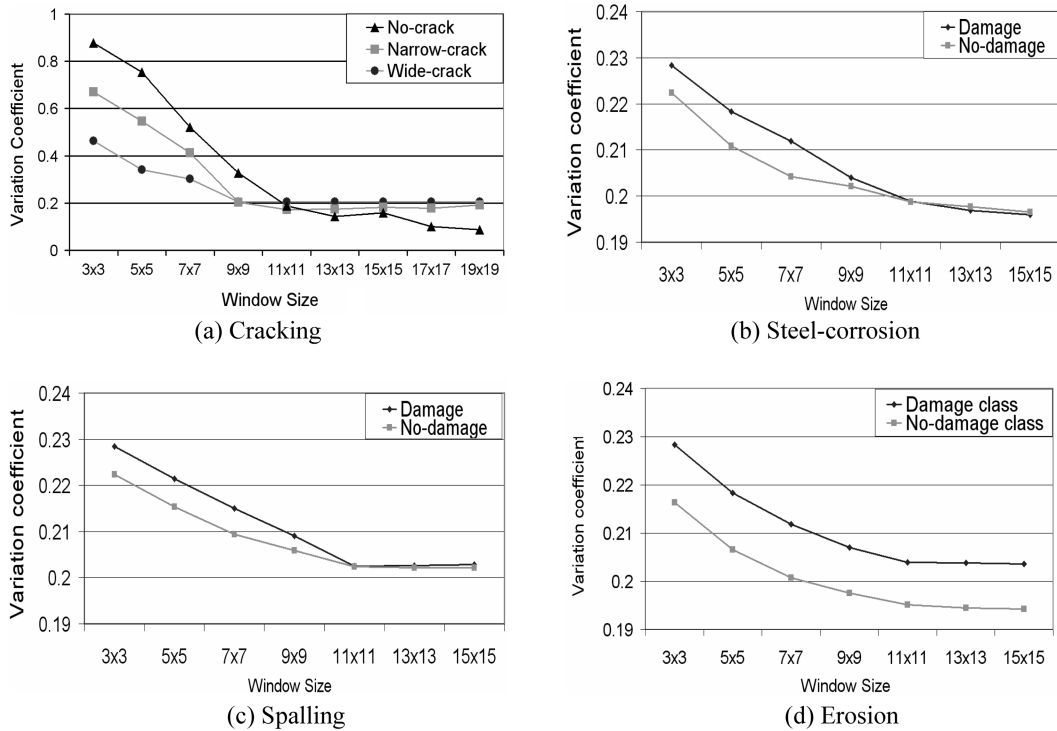


Fig. 6 Variation coefficients for the four types of damage

is too small or too large relative to the texture structure, then real textural properties will not be accurately reflected (Schowengerdt 1997). One method used to choose the appropriate window size is based on the calculation of the coefficients of variation for each object class (texture) as a function of the window size, using any given texture feature. The appropriate window size will be that for which the coefficients of variation start to stabilize for the majority of the object classes, while having the lowest value.

In this study, the homogeneity texture feature was randomly chosen for the calculation of the coefficients of variation for each class according to different window sizes. The coefficients of variation started to stabilize around the 9×9 window for the majority of the classes, for the image of the CANMET specimen C-3 containing cracking damage (Fig. 6(a)); for images of the other types of damage taken from field samples, stabilization occurred around the 11×11 window for most of the classes (Fig. 6(b-d)).

5.3. Selection of optimum features

The GLCM for each of the reconstructed images was calculated using a distance of 1 pixel, a direction of 0° between pixels, and a 9×9 pixel window in the case of the cracking images, and an 11×11 window for the other types of damage. Various second-order texture features can be derived from the GLCM (Haralick, 1979), however, many of them are redundant and capture similar concepts; features that do not help discrimination are discarded. The most effective texture features are selected through a process consisting of visual analysis, histogram analysis, and analysis of correlation matrices. In this study, the following second-order features were extracted from the GLCM: mean variance, homogeneity, contrast, entropy, second moment and correlation (Fig. 7).

The texture feature selection process was performed for each of the images in order to determine

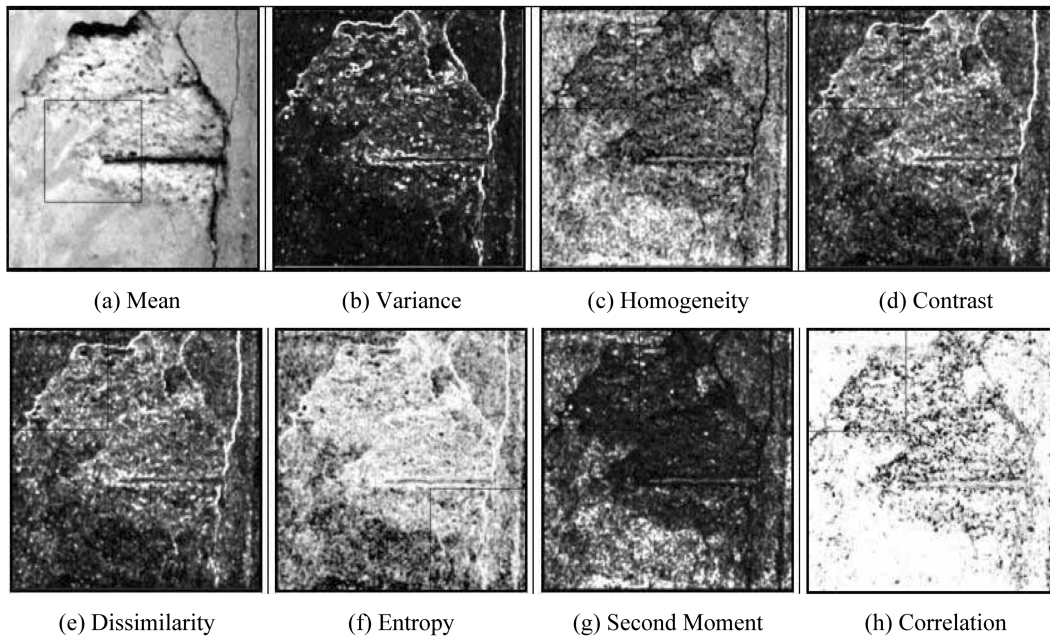


Fig. 7 Texture features extracted from GLCM of steel corrosion image

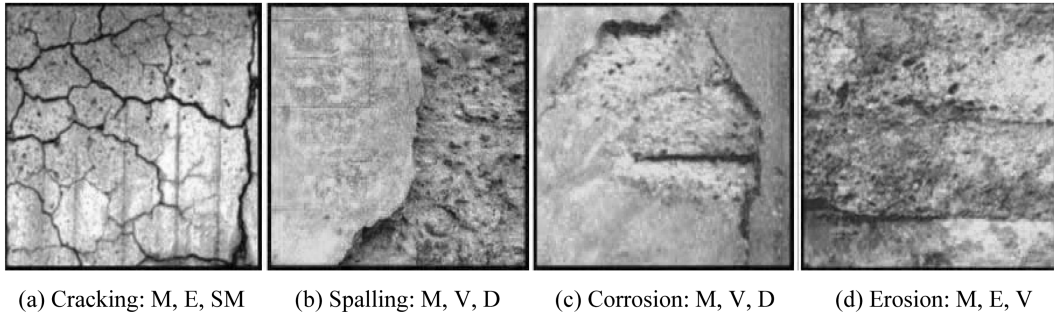


Fig. 8 Texture images composed of selected features for each type of damage

which texture features are most effective in distinguishing the various types of damage. For the cracking images, visual analysis of the texture features revealed that the contrast, correlation, entropy and variance texture features presented poor quality in terms of visual information. Display of the histograms indicated that three features, contrast, correlation, and variance, should be considered for elimination. Finally, the correlation matrix confirmed the removal of the contrast, correlation, dissimilarity, homogeneity, and variance features, due to their relatively high correlation. As a result, the mean, entropy, and second moment texture features were selected for this type of damage.

The same process conducted on images of the other types of damage resulted in the selection of the mean, variance, and dissimilarity features for the spalling images, the mean, entropy, and variance texture features for the erosion images and the mean, variance and dissimilarity features for the corrosion images. Texture images composed of the texture features selected for each of the four types of damage are presented in Fig. 8.

6. Classification

The textural information acquired through the GLCM analysis was combined with the spectral data and integrated into the classification process as input images, which consisted of the original greyscale image, along with the texture images produced using the selected texture features for the different types of damage.

There are two general approaches to the classification process: supervised and unsupervised classification. Supervised classification is closely controlled by the image analyst and requires previous knowledge of the data and of the classes desired. Unsupervised classification is more computer-automated and is dependent upon the data itself for the determination of the spectral classes; the analyst then identifies these classes after classification (Richards and Jia 1999). This study employs both supervised and unsupervised classification approaches in order to evaluate which of the two is more appropriate for applications in concrete damage analysis.

6.1. Maximum likelihood classifier

The maximum likelihood classifier (MLC) is a supervised classification technique that calculates the greatest probability that a pixel belongs to a given class, thus minimizing pixel misclassifications. In

order to train the MLC, training sites representing each object class are selected from the image to generate spectral signatures for these classes. The classifier then numerically compares each individual pixel in the whole image to these signatures and determines which class the pixel most likely belongs to; the pixel is then labelled accordingly and assigned a symbol or colour that relates it to that specific class. Verification sites are created for each class from areas on the image where the training sites were not produced; these sites are used to verify the accuracy of the classifications.

In this study, the MLC was used to characterize three classes of interest for crack images: no-crack, wide-crack, and narrow-crack; two object classes were used for the images of the other types of damage: no-damage and damage.

6.2. *K-means clustering*

The *K-means* unsupervised classification method is a clustering algorithm that groups pixels according to their spectral similarities based on statistics only, without any user-defined training classes. Classes of interest are defined by determining the optimal partitioning of pixels into the specified number of object classes. To perform the classification, the number of object classes is specified; heterogeneous regions of the image are then selected in order to give the classifier a sample of all the different classes of interest and their spectral variations. The classifier then locates the concentrations of spectrally similar pixels in the heterogeneous sample that are considered to represent classes in the image and are used to derive class signatures. When the clustering process is complete, pixels in each group are assigned a symbol or colour to show that they belong to the same spectral class or cluster.

In order to employ the *K-means* classifier, the number of object classes specified for the crack images was three, and for the other types of damage, the number of object classes selected was two.

7. Results and discussion

The results of the MLC and *K-means* classifications can be presented in a classified image, in which the pixels are displayed in the colour assigned to their associated class, and a cluster map,

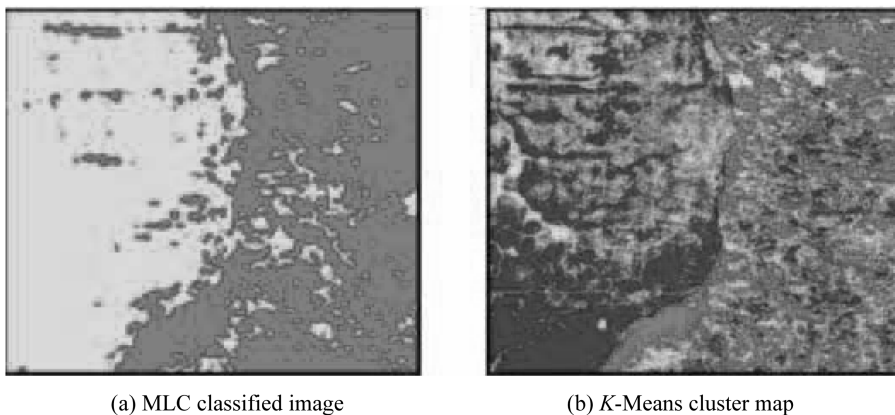


Fig. 9 Classifications of image of spalling damage from field sample

Table 2 Number and percentage of pixels per class in whole image for some of the classifications

Damage type	Classes	MLC		K-means	
		Number of pixels	% of pixels	Number of pixels	% of pixels
Cracking	No-crack	821035	78.3	793772	75.7
	Narrow-crack	149946	14.3	158335	15.1
	Wide-crack	77595	7.4	96469	9.2
Spalling	No-damage	558891	53.3	602931	57.5
	Damage	489685	46.7	445645	42.5
Corrosion	No-damage	640680	61.1	568328	54.2
	Damage	407896	38.9	480248	45.8
Erosion	No-damage	199229	19.0	171966	16.4
	Damage	849347	81.0	876610	83.6

which corresponds to the image that has been segmented, where pixels are represented by their symbol or colour. Fig. 9(a) is the classified image of spalling damage taken from the field sample and Fig. 9(b) is the cluster map of the same image.

Classifications can also be presented in a table that gives a statistical summary of the number and percentage of pixels in the whole image associated with each class. Results of the classifications for the cracking image, taken from CANMET C-3, and other types of damage, taken from field samples, are given in Table 2.

The final step of the classification is the evaluation of the accuracy of the results obtained, which indicates how well the classification performed. The overall result of the classification is presented in the form of a confusion matrix, from which many classification precision indexes can be calculated. It has been found that the most appropriate index to provide classification precision is the Kappa coefficient, because it takes account of all the elements of the confusion matrix (Fung and Ledrew 1988).

Table 3 presents the classification accuracies and Kappa coefficients for each class obtained by the MLC and the *K*-means classifier, for classifications of the CANMET C-1 cracking image and the field sample images of the other types of damage. The classification accuracies indicate that the *K*-

Table 3 Classification accuracies (%) for each class and Kappa coefficients for some classifications

Damage Type	Classes	MLC			K-means		
		Accuracy	Kappa	Overall	Accuracy	Kappa	Overall
Cracking	Wide-crack	78.4			72.9		
	Narrow-crack	76.6	0.78	78.6	70.7	0.69	71.3
	No-crack	79.1			73.2		
Spalling	Damage	77.5	0.75	76.8	74.6	0.73	74.8
	No-damage	78.9			75.2		
Corrosion	Damage	79.4	0.76	79.1	73.7	0.72	74.6
	No-damage	77.9			75.9		
Erosion	Damage	78.5	0.77	77.6	73.5	0.70	72.2
	No-damage	78.3			74.8		

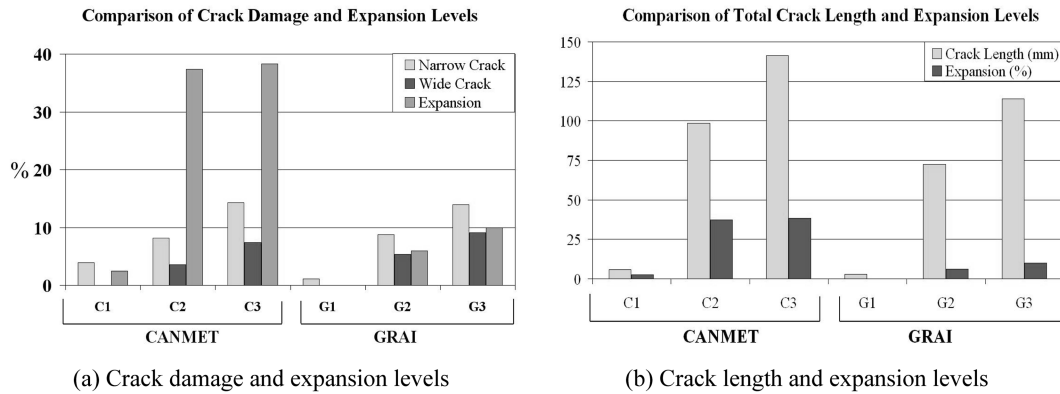


Fig. 10 Comparison of crack damage and expansion levels in CANMET and GRAI specimens

means classifier performed fairly well in all classifications, obtaining overall accuracies ranging from 71.3% to 74.8% and a Kappa coefficient range of 0.69-0.73. The MLC, however, performed better for every class compared with the *K*-means classifier, obtaining overall accuracies ranging from 76.8% to 79.1% and Kappa coefficients ranging from 0.75-0.78.

The overall MLC accuracy for the spalling damage classes, however, was slightly lower than anticipated; it was expected that this class would produce classification results closer to those of the corrosion damage class due to the similar textural appearance of the deterioration, which was also reflected by the fact that the texture feature selection process resulted in the same features for the two types of damage. The *K*-means classifier, though, did produce similar overall accuracies for these two types of damage, although the accuracies were lower than those obtained by the MLC. This may be an indication that for deterioration that has the same textural characteristics as spalling and corrosion damage, a clustering algorithm may be more appropriate for classification purposes.

Different quantitative evaluations can be done using the data contained in the statistical summary of the classifications, which essentially shows what percentage of the image contains concrete damage. Results of the MLC classifications presented in Table 2 reveal that the crack image has 7.4% wide cracks and 14.3% narrow cracks, totalling 21.7% crack damage; the spalling image has 46.7% damage, the corrosion image has 38.9% damage, and the erosion image has 81.0% damage.

Statistics from the classifications done for the CANMET and GRAI laboratory specimens were compared with the test measurements of the specimens; some correlation was noticed between the percentage of cracks and the average expansions, as demonstrated in Fig. 10(a).

Other quantitative analyses can be done upon conversion of the classified images into binary images; manual or automated methods can be used to sum pixels in order to calculate total crack-length or average crack widths. In this study, the total crack-lengths for the CANMET specimens were calculated to be 5.7 mm for C1, 98.6 mm for C2, and 141.3 mm for C3. Among the GRAI specimens, total crack-lengths were 2.9 mm for G1, 72.5 mm for G2, and 113.8 mm for G3. These values were compared with expansion levels in Fig. 10(b), which also demonstrated some correlation.

8. Conclusions

The approaches outlined in this study were effective in detecting and quantifying surface damage in concrete, such as cracks, spalling, corrosion, and erosion, from greyscale imagery. The use of Harr's wavelet transform along with the GLCM texture analysis effectively reduced the amount of unwanted texture information usually present in concrete imagery. This allowed for the extraction of more representative texture features to characterize the classes of interest, which in the case of this study, consisted of the different types of concrete damage. Determination of the optimum texture features for the different types of damage provided understanding of which features work best for the various types of damage. Although the unsupervised *K*-means classifier produced slightly lower classification accuracies compared to the supervised MLC technique, it may be more appropriate for applications involving concrete imagery of certain types of deterioration, such as spalling and corrosion. In addition, unsupervised classifications are not dependent upon information from the analyst in order to determine the spectral classes within the image, which may result in a more automated system.

Since these methods can provide more cost- and time-effective evaluations compared with traditional visual inspections, assessments can be carried out more often to supplement visual assessments. These techniques are also suitable for quantitative evaluations, such as total amount of surface damage, total length of cracks, and range of crack-widths, which can improve the quality of concrete condition information used for making decisions concerning maintenance and repairs. For further studies these approaches can be evaluated for their potential to be used as part of a monitoring system for concrete structures, such as bridge decks and highway infrastructures. The quantitative analysis resulting from these approaches can also be used in the development of an automated system for damage assessment to determine the different types and levels of deterioration, from a collection of concrete images, for classification according to the level of surface damage. Another study can focus on the use of the IR thermography method; the advantage of this approach is that images can be acquired at night, which would cause even less traffic disruption.

Acknowledgements

This study was supported by grants from the Fonds québécois de recherche sur la nature et les technologies (FQRNT) and from the Natural Sciences and Engineering Research Council of Canada (NSERC). The authors wish to thank the Centre de recherche sur les infrastructures en béton (CRIB) for its valuable contribution to this study.

References

- Bettigole, N. and Robison, R. (1997), "Bridge decks: design, construction, rehabilitation, replacement", ASCE press; p. 5.
- Carino, N. J. (2003), "Non-destructive test methods to evaluate concrete structures", *Proceedings of the 6th CANMET/ACI Int. Conf. on Durability of Concrete*, Thessaloniki, Greece, June, 1-78.
- Fournier, B. and Bérubé, M. A. (2000), "Alkali-aggregate reaction in concrete: a review of basic concepts and

- engineering implications”, *Canadian J. Civ. Eng.*, **27**, 167-191.
- Fung, T. and Ledrew, E. (1988), “The determination of optimal threshold levels for change detection using various accuracy indices”, *Photogrammetric Engineering and Remote Sensing*, **54**(10), 1449-1454.
- Gaudreault, M. (2000), “The St. Lawrence Seaway (Québec, Canada): a case study in the management of structures affected by alkali-aggregate reaction”, *Proceedings of the 11th Int. Conf. on AAR in Concrete*, Québec City, June, 1293-1302.
- Haralick, R. M. (1979), “Statistical and structural approaches to texture”, *Proceedings of the IEEE*, **67**(5), 786-804.
- Kabir, S., He, D. C. and Rivard, P. (2006), “Urban classification of high resolution IKONOS imagery using texture”, *Proceedings of Joint Int. Conf. on Computing and Decision Making in Civil and Building Engineering*, Montréal, June, 326-335.
- Kiema, J. B. K. (2002), “Texture analysis and data fusion in the extraction of topographic objects from satellite imagery”, *Int. J. Remote Sensing*, **23**(4), 767-776.
- Richards, J. A. and Jia, X. (1999), *Remote Sensing Digital Image Analysis: An Introduction*, Springer-Verlag, New York.
- Rivard, P. and Ballivy, G. (2005), “Assessment of the expansion related to alkali-silica reaction by the damage rating index method”, *Construction and Building Materials*, **19**(2), 83-90.
- Schowengerdt, R. A. (1997), *Remote Sensing: Models and Methods for Image Processing*, Academic Press, San Diego.
- Scott, M., Rezaizadeh, A., Delahaza, A., Santos, C. G., Moore, M., Graybeal, B. and Washer, G. (2003), “A comparison of nondestructive evaluation methods for bridge deck assessment”, *NDT&E Int*, **36**, 245-255.
- Shaban, M. A. and Dikshit, O. (2001), “Improvement of classification in urban areas by the use of textural features: the case study of Lucknow City, Uttar Pradesh”, *Int. J. Remote Sensing*, **22**(4), 565-593.